JOURNAL OF AEROSPACE COMPUTING, INFORMATION, AND COMMUNICATION
Vol. 7, March 2010

Optical Wireless Links for Intra-Satellite Communications: Reflection Models and Hardware Optimization

Remo Tamayo
Instituto Nacional de Técnica Aeroespacial

José Alonso
Universidad Complutense de Madrid

and

Juan José Jiménez, Ignacio Arruego, and Héctor Guerrero*
Instituto Nacional de Técnica Aeroespacial

DOI: 10.2514/1.30271

The present work is a study on the propagation channel (physical layer) for wireless infrared communications in intra-satellite environments. Substituting cables and connectors with optical links inside a spaceborn platform offers many advantages and represents some technical challenges. We show analytical calculations, simulations, and experimental results for reflection models for aerospace materials, as well as wavelength division multiple access techniques for channel multiplexing. Improvements in the selection and optimization of emitter–detector pairs are also presented.

I. Introduction

A. History and Motivation of intra-Spacecraft Optical Wireless Communications

OPTICAL diffuse wireless communications are used in a wide variety of environments. They have been studied extensively in office environments. They were first proposed by Gfeller and Bapst [1]. In many situations, infrared (IR) radiation is preferable to radiofrequency (RF) in wireless communications. Some of the advantages of IR over RF are availability of unregulated bandwidth and immunity to interference, which guarantees the absence of electromagnetic incompatibility. IR radiation behaves (in the 800–1000 nm band, used for OWLS) very much like visible light: it is absorbed by dark surfaces, diffusely reflected by light surfaces, and specularly reflected by polished surfaces. Last but not least IR radiation does not propagate through walls, which makes it possible to have multiple subnets in separate compartments without interferences [2].

The application of optical wireless links to intra-spacecraft (OWLS) communications was proposed for intra-satellite applications in the 1990s [3,4]. Since 1999, several projects have been funded by the European Space Agency (ESA) to study and validate these technologies, that have also been flown in the NANOSAT-01. This satellite, developed by INTA, was launched on 18 December 2004 onboard Ariane V as a secondary payload of the Helios 1B satellite. Also, OWLS technologies were demonstrated in FOTON M3. The full OWLS history has recently been written [5].

There are several reasons for the usefulness of this technology in a spacecraft environment. The first one is weight reduction, as a consequence of the removal of communication connectors and cables. In this connection, further

Received 15 March 2007; accepted for publication 30 December 2009.
* guerreroph@inta.es

benefits in weight reduction are related to launch costs and fuel requirements, such that the removed harness can be replaced by additional payloads. Beyond these advantages, integration and test activities may also benefit from wireless systems: real-time monitoring of data traffic without traditional break-out-boxes is possible; connector savers or connection/disconnection control sheets are no longer needed (the number of connections/disconnections of a flight connector is very low, each use reduces its lifespan); routing of the remaining harness is easier, etc. The absence of cables, furthermore, provides greater mobility when moving instruments (telescopes, sensors, deployable mechanisms, etc.) which are then free from movement restrictions imposed by cables and connectors. The possibility of introducing last-minute design modifications is another advantage worth taking into account. Lastly, AIT (assembly, integration, and test) tasks are remarkably simplified. A technology that dispenses with the use of communication connectors is always welcome. Another reason for the usefulness of OWLS, with respect to other wireless technologies (i.e. RF), is the absence of electromagnetic incompatibility in onboard optical channels. Optical transmission of data is neither "invasive" from the electromagnetic compatibility (EMC) point of view, nor does it create electromagnetic interferences (EMI). The "cleanliness" of this technology in the EMC/EMI aspects makes it especially suitable for aerospace applications. In summary, OWLS will open a new world of opportunity for future interconnections inside spacecrafts, besides reducing the time and risk in such a critical phase in the development of a spacecraft, as is the AIT.

B. OWLS Basics

Schematically, an optical wireless communication channel consists of an emitter and a detector which are not connected by means of cables or optical fibers. Both emitter and detector are placed inside a closed environment, in which light is transmitted from the emitter to the detector.

Emitters are usually IREDs (infrared emitting diodes), although LEDs (light emitting diodes) and LDs (laser diodes) can also be used. The emitter diffuses IR radiation in the environment. Radiation is reflected (diffusely or specularly) on the walls and other devices of the channel, and finally arrives to the detector. If there is a straight optical path that links the emitter and the detector, then we talking about a LoS (line of sight) optical channel. If no such optical path exists, then we define the channel as a diffuse (or quasidiffuse, when there is a reflective repeater in the channel) system (Fig. 1).

There are many different modulations, but for our purposes we will study one of the simplest: OOK (on–off keying), which represents digital data by the presence or absence of the carrier wave. In the simplest implementation

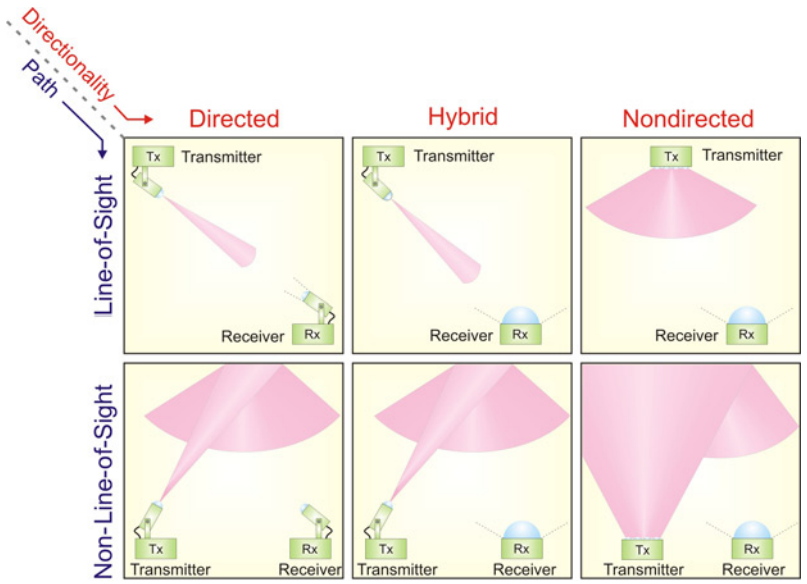

Fig. 1 Schemes for OWLS communications.

of the OOK modulation, the presence of radiation in the detector during the specific length of a bit represents a "1", while its absence represents a "0". Of course, more complex modulations exist and are widely used, but they are not significant for the purpose of the problems dealt with here.

C. Objectives

Since, so far, there is no algorithm that provides optimal positions and orientations for emitters and detectors, given the geometry of the environment, our main task has been to improve the functioning of some aspects of the system. In order to do this, we have divided the study of the channel in three parts: channel simulation reflection models, optical filters for WDMA (wavelength division multiple access), and detector optimization.

II. Simulations

A. Reflection Model

Two main factors affect the quality of an optical link: power distribution and bandwidth. Given the way an optical channel is constructed, it is unavoidable that two rays emitted simultaneously reach the detector at different times, due to the differences in their optical paths. This difference in time of flight causes an emitted bit of length t_0 to be received as having a length of $t_0 + \Delta t$. In Fig. 2 this broadening of the bit can be appreciated for several bit shapes.

This broadening of pulses due to multipath effects imposes the main limitation on the system bandwidth. Other limiting factors are the bandwidths of the emitters (LEDs or IREDs) and detectors (PIN Silicon photodiodes, in our system). Emitters are pulsated in OOK modulation schemes. The emitter must be able to switch on and off fast enough for individual bits to be distinguished.

In order to modify the geometry for the system to comply with the specifications, an accurate estimation of the bandwidth is needed. To characterize the bit broadening we will use the impulse response of the system. Impulse response for a spatial location of the optical channel is defined as the signal received by a detector, as a function of time when the emitter, placed somewhere else inside the environment, emits an instant pulse of radiation (mathematically represented by a Dirac Delta). As long as signals are considered to be time-invariant, the received signal obtained will be the convolution of the emitted signal with the impulse response of the system.

Simulation, by means of ray tracing using Monte Carlo methods, has proven to be a very valuable tool in predicting both power distribution and impulse response of wireless optical links [6–9], although for simple geometries (environments), the impulse response can be computed analytically.

To predict power distribution and impulse response, we also need a good model of light scattering by the different surfaces in the environment (see Fig. 3). Because of this, a precise angular diffusion characterization of all the materials in the channel is critical. Simple reflection models, which consider reflections on materials as either purely specular or Lambertian, are insufficient for the correct characterization of an optical environment. In most part of the scientific literature, materials are supposed to be Lambertian, since office environments have carpets, unvarnished wood, and plaster walls which acceptably comply with the Lambertian model [10]. In space environments, however, most of the surfaces are covered with space paints which have a nonnegligible amount of specular components, and materials such as Kapton or Mylar, which are clearly non-Lambertian.

The Lambert model assumes that the radiance of the light scattered on a diffusive surface is constant. Very few materials exhibit this behavior (barium sulfate is one of them, largely used in integrating spheres). A more realistic model for many standard materials is Phong [11], which characterizes the surface scattering of light by means of three components: scattering from undirectional ambient light, Lambertian scattering from point sources, and partial scattering from point sources along the reflection direction. The Phong model, as will be seen, is able to characterize space environment materials with much more accuracy than the Lambertian model.

Let us consider the patch of a surface receiving radiation from a direction $\vec{u}$. We will call $E(\vec{u})$ the corresponding irradiance on this patch and $L(\vec{v})$the reflected radiance along the direction $\vec{v}$. The surface reflectance is fully characterized by the bidirectional reflectance distribution function (BRDF) which is defined as follows:

$$f_r(\vec{u}, \vec{v}) = \frac{L(\vec{v})}{E(\vec{u})} \tag{1}$$

The Phong model lacked a physical basis, and it was not formulated as a BRDF. Lewis [12] introduced a modified Phong model physically plausible, which can be written as the sum of a diffuse component (the Lambertian diffusion)

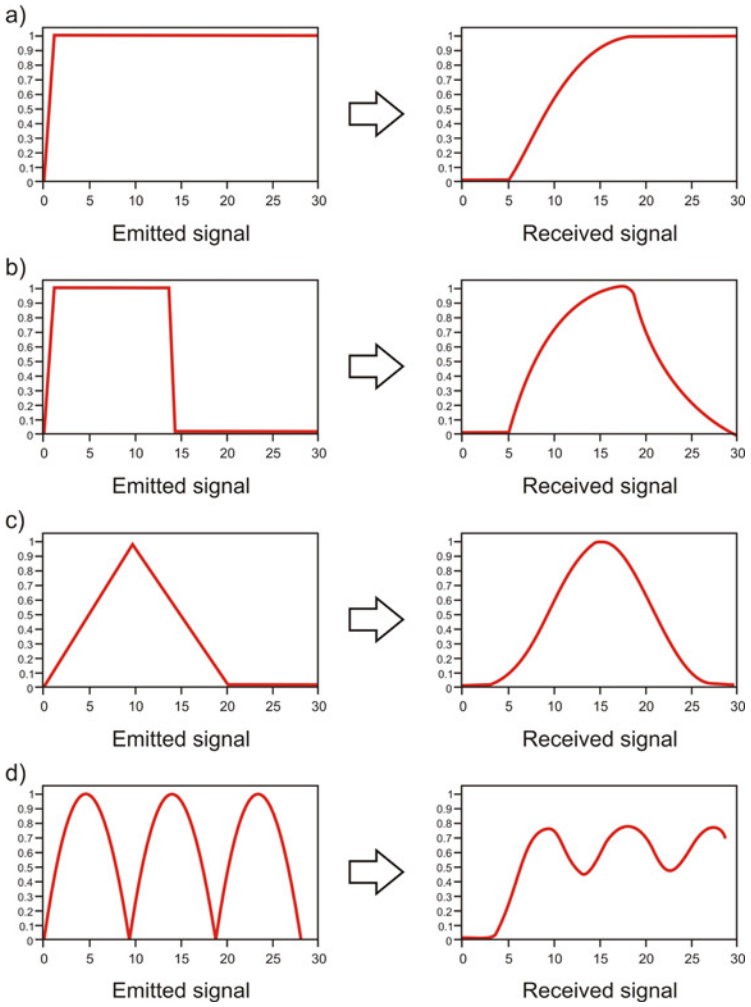

Fig. 2 Examples of several signal profiles when emitted and detected through a generic optical channel. Multipath dispersion causes broadening in the pulses. In the last case (d), this broadening is responsible for the overlapping of pulses. The system would have reached its bandwidth limit.

and a specular component, that we will refer to as the Phong component:

$$f_r(\theta, \alpha) = k_D \frac{1}{\pi} + k_S \frac{n+2}{2\pi} \cos^n \alpha \tag{2}$$

In this model, the surface reflectance is assumed to be isotropic, so the incidence and reflectance directions are characterized by the angle made by the incident radiation with the normal surface, θ, and the angle between the specular direction and the observation direction, α. Here k_D and k_S are, respectively, the diffuse and specular reflectivity, the fractions of energy that are diffusely and specularly reflected. The exponent n is chosen to fit the distribution of energy reflected around the specular direction. The larger the value of n, the sharper the specular reflection; Phong components with a large n will model low-scattering, as reflection produced on partially or totally polished surfaces. The modified Phong model by Lewys does not consider the ambient term of the original Phong model. In our application, this is not a limitation because there is no ambient light in satellite environments. The polar plots of the radiance corresponding to the Lambert and Phong components and the full model are shown in Fig. 3.

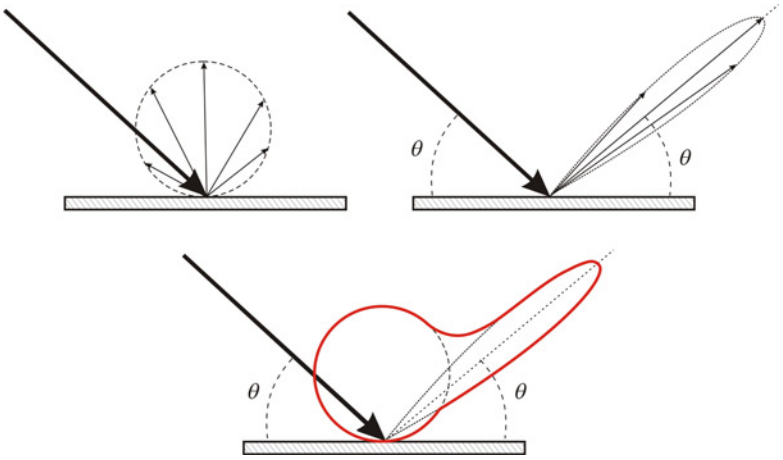

Fig. 3 Schematic representation of the angular distribution of reflected power in the Lambert (top left) and the Phong without diffuse component (top right) models. Combination of both components yields Phong complete angular distribution (bottom). Since most of the space materials, such as Kapton, space thermal paints, or multilayer insulators (MLIs) exhibit clear non-Lambertian behavior and these materials account for most of the available surfaces in the intra-spacecraft environment, materials must be well characterized in order to achieve accurate simulations.

There are many other models for surface reflectance obtained both from experimental reflectance measurements on samples and from theoretical derivations from surface roughness models. In particular, some rough surfaces are suitable for generalized Lambert models [13], for which $f_r = k(\cos\theta\cos\alpha)^m$, k being a constant and m the Lambert mode. Nevertheless, in satellite applications the modified Phong model is better suited, in particular the Phong component, as we will show in the following sections.

B. Emitter Characterization

Most of the emitters suited for OWLS systems are LEDs or IREDs. The emission from the active surfaces of these semiconductor device is well approximated by a Lambertian illumination pattern. Nevertheless, the radiance pattern of a particular solid-state emitter device depends heavily on the characteristics of its package. The presence of collimating optics is especially important, given that it usually produces a more directional emission pattern. As part of a general study on OWLS hardware, tens of LEDs and IREDs were characterized. Two of the angular spectra of these emitters are shown in Fig. 4. To measure these radiation patterns, the emitters were placed on a rotating platform with a constant angular speed. A detector connected to an oscilloscope was placed in front of the platform. The platform completed two turns within a sweep of the scope time axis, so two intensity maxima were recorded. These maxima were 2π radians apart; thus, by using relative measurements we were able to calculate the angles for which power decayed to 50% and 5%. In OWLS applications, the wide radion pattern of the Vishay 3700 in Fig. 4(left) is preferable to the narrower patterns of lensed IREDs (Fig. 4(right)). We then assumed the emitter to be Lambertian in the model we present hereafter.

C. Model of the Wireless Optical Channel and Results

The optical channel is modeled by a source and a receiver contained in a closed environment that allows light propagation by means of reflections in the walls and components placed in the channel. The source is a LED or IRED emitting a time-dependent radiant flux $\Phi(t)$ and the receiver is a PIN photodiode with responsivity s, and working in a direct detection mode. The received signal $R(t)$ is thus given by

$$R(t) = s\Phi(t) \otimes h(t) + N(t) \tag{3}$$

where $\otimes$ represents a convolution, $h(t)$ is the impulse response of the system, and $N(t)$ is the ambient illumination (noise). Ambient noise in a satellite is negligible, so we will not include it in our calculations.

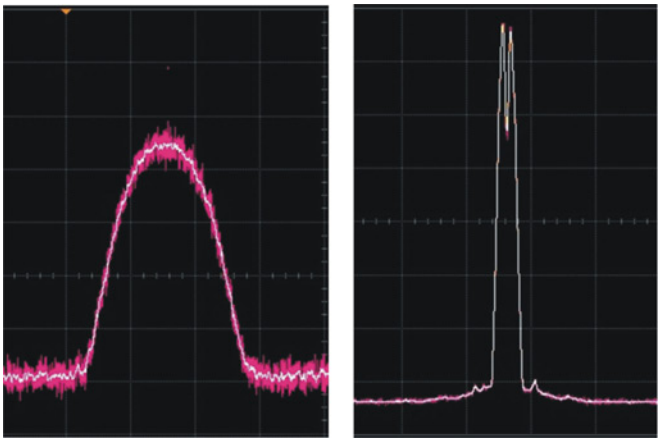

Fig. 4 Examples of angular emissivity for two IREDs. One of them can be approximated by a Lambertian emission function (Vishay 3700, left), ant the other one cannot (Vishay 6200, right). The model on the right had a soldering point which shaded the emission at 0°. Simulation of emitters of this type must be done by means of tabulated values and interpolation, rather than by adjust functions.

The surface of the photodiode is much smaller than the surface of the walls, so we can assume that the incoming radiance is constant over the entire photodiode surface. This is equivalent to considering the photodiode as point-like. This approach can lead to errors in the impulse response calculation when there is a LoS between the emitter and the detector, since a Dirac Delta in the emitter would be transformed into a Dirac Delta in the detector. But in a totally diffusive environment with no LoS, calculations with point-size and extensive detectors yield the same results, provided that the detector is much smaller than the channel environment. Calculations, on the other hand, are much more complex when assuming extensive detectors.

It can also be noted that, unlike RF, the detectors for IR communications are thousands of times greater than the wavelength of the incoming radiation. This means that IR systems do not suffer multipath shading, unlike RF systems. Optical transmissions are modulated in intensity, not in phase (coherent light is not used). Therefore, we can consider that if the emission $E(t)$ is constant in time, then $R(t)$ will also be constant, and thus all the parameters in the channel will be constant [10], that is, the channel behaves as a time-invariant linear system.

As stated above, analytical calculations are impractical in complex systems. Nevertheless, it is possible to carry them out in simple geometry environments, in order to validate the models and the simulations. To perform an analytical calculation, the simple cylindrical environment shown in Fig. 5 was chosen. Rays from the emitter bounce once from the wall and reach the detector. No LoS is considered, only a purely diffuse transmission.

The cylinder has length L and radius H. The emitter and detector are located at the center of the planar faces of the cylinder, with a baffle avoiding LoS. We will use the coordinates x and φ to locate a point on the inner surface of the cylinder. Let us consider the surface patch with area $\mathrm{d}A = H\,\mathrm{d}\varphi\,\mathrm{d}x$. The irradiance on this patch is given by

$$E(x,\varphi) = \frac{I(\hat{\theta})\mathrm{d}\Omega}{\mathrm{d}A}$$

where $\mathrm{d}\Omega = \mathrm{d}A\cos\theta/(x^2+H^2)$ is the solid angle subtended by the patch, and $I(\hat{\theta})$ is the radiant intensity of the emitter (which is assumed to be symmetric and independent of angle φ). The radiance reaching the detector from the same patch is, according to the definition of the BRDF,

$$L(x,\varphi) = f_r(\theta(x),\alpha(x))E(x,\varphi)$$

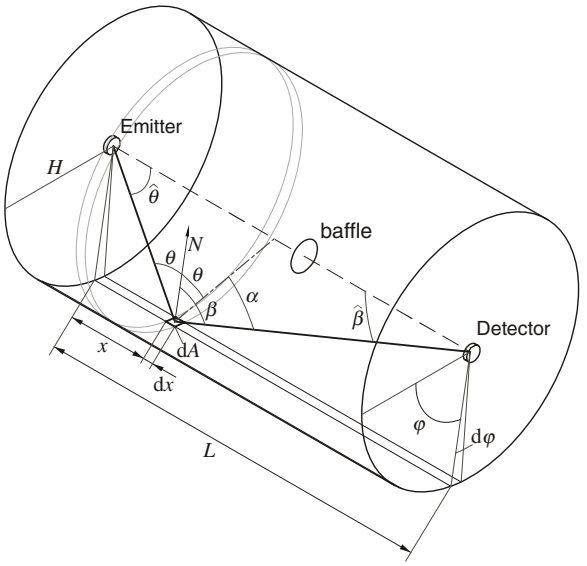

Fig. 5 Schematic view of the cylinder on which calculations have been performed.

as the angles θ and α depend on the impact coordinate x along the cylinder axis, but do not depend on the angular coordinate φ. Substituting the previous equations and using the modified Phong model, we obtain

$$L(x,\varphi) = k_D \frac{I(\hat{\theta})}{\pi(x^2+H^2)} \cos\theta + k_S \frac{(n+2)I(\hat{\theta})}{\pi(x^2+H^2)} \cos\theta \cos^n\alpha \tag{4}$$

Factor (x^2+H^2) in the denominator accounts for the reduction of the surface irradiance because of the inverse squared distance law. As we are assuming the emitter to be Lambertian, $I(\hat{\theta}) = (P_0/\pi)\cos\hat{\theta}$, where P_0 is the total flux (or power) emitted by the source, using the relation $\cos\theta = H/\sqrt{x^2+H^2}$, we can express the radiance as follows:

$$L(x,\varphi) = \frac{P_0}{\pi^2 H^2} \cos^3\theta \cos\hat{\theta} \left[k_D + k_S(n+2)\cos^n\alpha\right] \tag{5}$$

The flux (power) reaching the detector from the patch at coordinates $(x,\ \varphi)$ is given by $\mathrm{d}\Phi_d(x,\varphi) = L(x,\varphi)\cos\hat{\beta} S_d\,\mathrm{d}\Omega_d$, where S_d is the area of the detector and $\mathrm{d}\Omega_p = \mathrm{d}A\cos\beta/((L-x)^2+H^2)$ is the solid angle subtended by the patch from the detector position. The power coming from all the patches with the same x coordinate is

$$\mathrm{d}\Phi_d(x) = S_d \int_{x=\text{constant}} L(x,\varphi)\cos\hat{\beta}\,\mathrm{d}\Omega_d = \frac{2\pi H S_d L(x)\cos\hat{\beta}\cos\beta}{(L-x)^2+H^2}\mathrm{d}x \tag{6}$$

and the power reaching the detector per unit length along the cylinder, $P_d = \mathrm{d}\Phi_d/\mathrm{d}x$,

$$\begin{aligned} P_d &= \frac{2P_0S_d}{\pi H^3}\cos^3\theta\cos^3\beta\cos\hat{\theta}\cos\hat{\beta}[k_D + (n+2)k_S(\cos\alpha)^n] \\ &= \frac{2P_0S_dH^3x(L-x)}{\pi(x^2+H^2)^2[(L-x)^2+H^2]^2}\left[k_D + (n+2)k_S\left(\frac{H^2+x(L-x)}{\sqrt{x^2+H^2}\sqrt{(L-x)^2+H^2}}\right)^n\right] \end{aligned} \tag{7}$$

where we have also used $H^2 = \cos^2\beta[(L-x)^2+H^2]$. In a stationary regime, the total flux reaching the detector (per unit area of detector surface) is obtained by integrating the radiance over the whole span of variables x and φ. However, to compute the impulse response of the optical channel, we have to take into account that the flight time

of each ray depends on the coordinate x. The flight time for each ray from the emitter to the detector depends on the ray trajectory:

$$\tau(x) = \frac{1}{c}\left(\sqrt{x^2 + H^2} + \sqrt{(L-x)^2 + H^2}\right) \tag{8}$$

The shortest trajectory corresponds to the midpoint of the cylinder, $x = L/2$. The time of flight is symmetric with respect to this position, and reaches maximum values at $x = 0$ and $x = L$. All the light reaches the detector within the interval $[\tau_{\min}, \tau_{\max}]$, where $\tau_{\min} = \tau(L/2)$ and $\tau_{\max} = \tau(0) = \tau(L)$. Because of this behavior, $x(\tau)$ is a bivaluated function. Equation (8) can be inverted with the result:

$$x_{1,2}(\tau) = \frac{L^3 - L\tau^2 \pm \tau\sqrt{(L^2 - \tau^2)(4H^2 + L^2 - \tau^2)}}{2(L^2 - \tau^2)} \tag{9}$$

where the plus is used for subscript "1" and the minus is used for subscript "2". For each time of flight in the interval $[\tau_{\min}, \tau_{\max}]$, there are two symmetrical positions x_1 and x_2, for which the rays reach the detector at the same time. The impulse response at any time $t \in [\tau_{\min}, \tau_{\max}]$ is then

$$h(t) \propto P_d(x_1) + P_d(x_2) \tag{10}$$

By direct substitution of (9) into (10), we may compute the impulse response analytically.

The impulse responses computed by means of Eq. (10) are shown in Fig. 6. The three plots to the left show the impulse response in a long cylinder with $L = 900$ mm and $H = 100$ mm. The three plots to the right show the impulse responses for a shorter cylinder with $L = 200$ mm and $H = 100$ mm. Each plot contains three graphs, computed assuming the diffusion is only Lambertian ($k_S = 0,\ k_D = 1$), only specular with some diffusion ($k_S = 1,\ k_D = 0$) or a mixture of both ($k_S = 0.5, k_D = 0.5$). For Lambertian diffusion, the surface of the cylinder reflects more light at $x = 0$ and $x = L$, that is, at the end of the time interval ($t = \tau_{\max}$). Nevertheless, the low emission and irradiance of the emitter and the detector at those extreme angles softens the impulse response and makes it have a maximum near the midpoint of the time interval. The Phong component is more intense at the specular direction, that is at $x = L/2$, which coincides with the shortest flight time. For this reason, a maximum at $t = \tau_{\min}$ is to be expected. For large values of n, we indeed observe this clear maximum at the shortest flight time. But for $n = 1$ (that is, large diffusion at the specular direction), and because of the lack of symmetry of the cosine functions, the maximum of the impulse response can be displaced to the right, especially for long cylinders.

As can be seen in the figures, the reflection model plays an essential role in the impulse response of the system, and hence it is critical for the bandwidth of the optical wireless link.

D. Channel Parameters

There are some figures of merit which characterize the optical link, that directly depend on the impulse response: the optical path loss (OPL), the mean delay (μ), and the rms delay spread (D).

For a diffuse channel with impulse response $h(t)$ and an emitted power $P_0(t)$, the average emitted power is defined as:

$$P_{tx} = \lim_{T\to\infty} \frac{1}{2T} \int_{-T}^{T} P_0(t)\,\mathrm{d}t \tag{11}$$

For that average emitted power, the average received power at the detector is

$$P_{rx} = G_0 P_{tx} \tag{12}$$

where G_0 is the optical gain, defined as follows:

$$G_0 = \int_{-\infty}^{\infty} h(t)\,\mathrm{d}t \tag{13}$$

The OPL of the channel is defined from the optical gain:

$$\mathrm{OPL} = -10 \log G_0 \tag{14}$$

Kahn et al. [10] proposed that only two parameters are enough to characterize the main features of an optical communications channel: the mean delay (μ) and the rms delay spread (D). The first one is the first moment of the

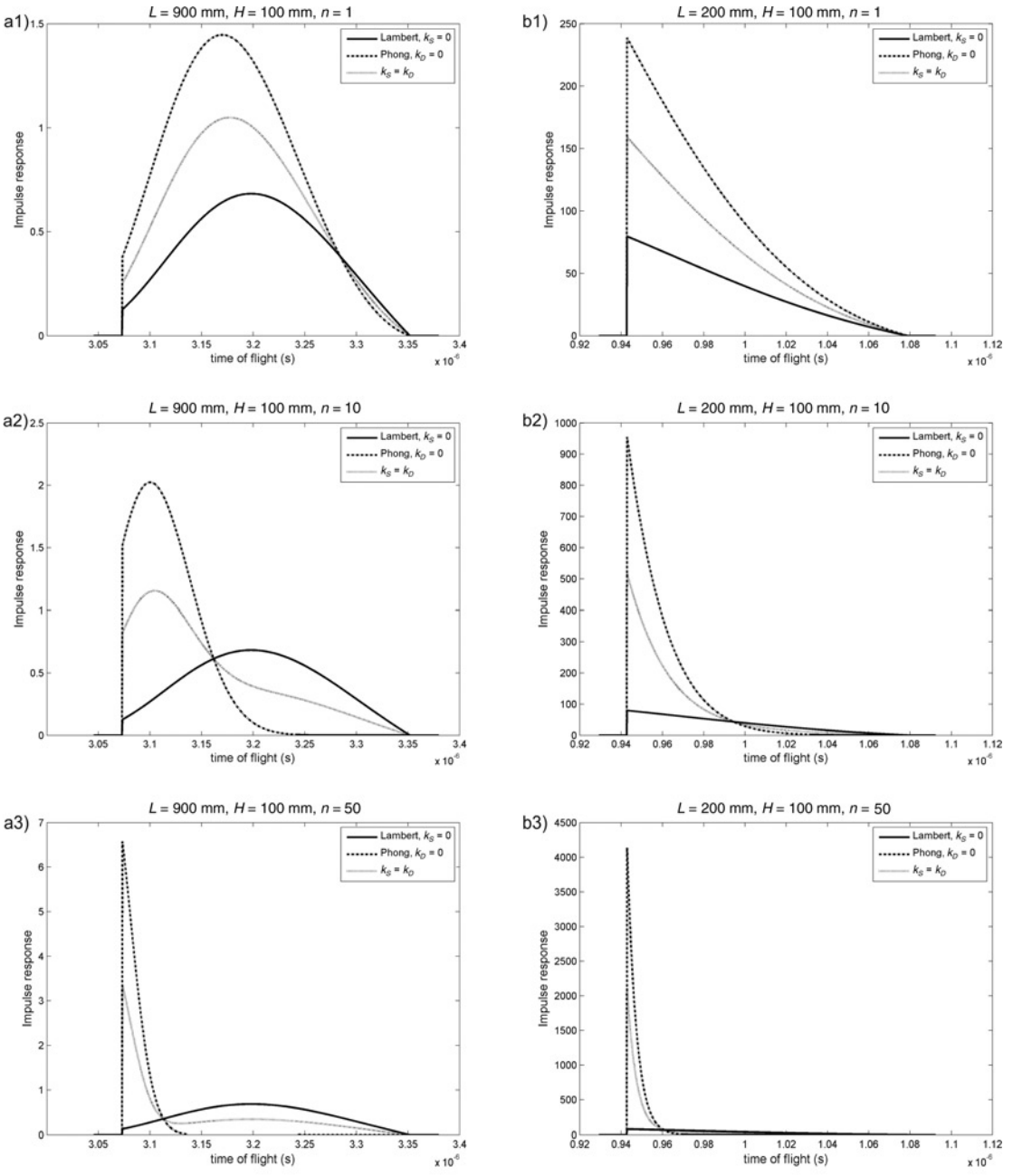

Fig. 6 Impulse responses of a wireless optical channel inside a cylinder with radius $H = 100$ mm and length (a) $L = 900$ mm, (b) $L = 200$ mm. In each plot the impulse responses for pure Lambertian reflection, specular Phong reflection with exponent n and a mix of them, are presented: (a1, b1) $n = 1$; (a2, b2) $n = 10$; (a3, b3) $n = 50$.

square of the impulse response of the channel:

$$\mu = \langle t \rangle_{h^2} = \frac{\int_{-\infty}^{\infty} t\, h^2(t)\, \mathrm{d}t}{\int_{-\infty}^{\infty} h^2(t)\, \mathrm{d}t} \tag{15}$$

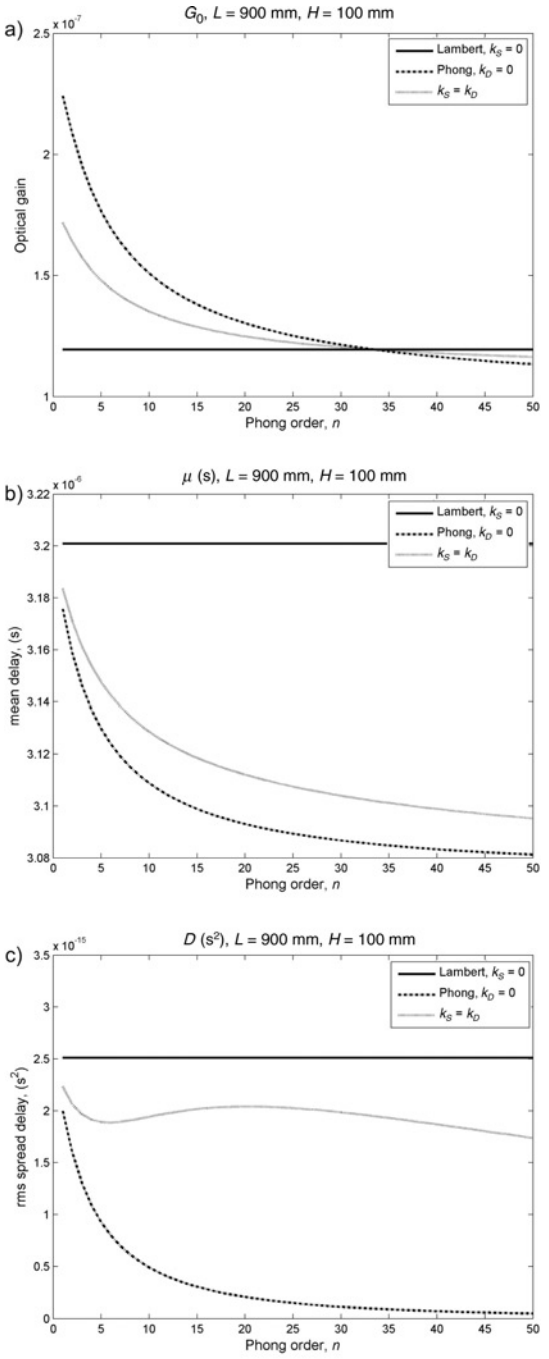

Fig. 7 Optical gain (a), mean delay (b) and rms spread delay (c) for a wireless optical link inside a cylinder with a height of 900 mm and a radius of 100 mm.

The second one is the width of the square of the impulse response:

$$D = \langle (t-\mu)^2 \rangle_{h^2} = \langle t^2 \rangle_{h^2} - \mu^2 = \frac{\int_{-\infty}^{\infty} (t-\mu)^2 h^2(t)\,\mathrm{d}t}{\int_{-\infty}^{\infty} h^2(t)\,\mathrm{d}t}$$

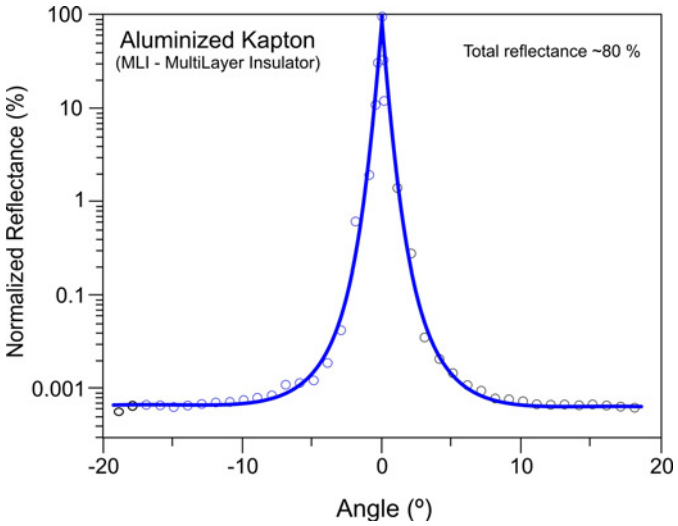

Fig. 8 Reflectance variation as a function of angle for a MLI. Angles show differences between observation angle and specular direction. The greatest reflected power is in the specular direction.

The parameters G_0, μ, and D are presented in Fig. 7 for a cylinder with a length $L = 900$ mm and a radius $H = 100$ mm. The three parameters have been computed as a function of the Phong order n. The Lambert diffusion does not depend on n, and so it is represented as a horizontal line. The reflection model with a higher gain is the specular reflection with a low-diffusion coefficient. The delay (both mean and rms) is greater with a Lambert reflection model. Both the mean delay and the rms spread delay are smaller for highly specular reflection. This can be seen in Fig. 6.

E. Materials Characterization

After verifying that different models have very different predictions, we characterized a frequently used space material: a MLI that is composed by a stack of layers of aluminized kapton. The MLI measured was space-grade (supplied by Alcatel Space France). Reflected power was measured as a function of the observation angle for this material. Results are shown in Fig. 8. The behavior is markedly non-Lambertian.

When fitting data shown in Fig. 8 to Eq. (2), the Phong term was $\cos^{61}(\theta)$, a very high exponent that agrees with previous works [14]. The behavior of MLIs is mostly specular with a slight Lambertian component around the specular direction. We concluded that this kind of materials used in space applications cannot be simulated using the Lambertian model which is widely used when simulating office environments for wireless local area networks applications.

III. WDMA

A satellite, base camp for OWLS technologies, has several hardware systems and subsystems connected among themselves and with the OBDH (on board data handling) subsystem. Every subsystem must have an independent communication channel with the OBDH, that is, in order to operate on separate networks. There are several methods for achieving multiple access in optical wireless channels. Some of these methods are "electronic", such as TDMA (time division multiple access), FDMA (frequency division multiple access), or by means of codes CDMA (code division multiple access). Optical techniques can be physical or spatial separation of the subsystems SDMA (space division multiple access) or WDMA, which is the technique studied in this paper. WDMA allows several channels to transmit simultaneously and without interference by means of wavelength separation. FDMA has been previously used in demonstrators of OWLS technologies, but is beyond the scope of this work [5].

First, experiments were conducted using three emitters centered in the visible (LED) and in the near infrared (IRED), with peak emission wavelengths centered at 660, 810, and 950 nm. Solutions based on laser emitters could

be an easier solution (spectrum width of nm instead several tens of nm) [15]. However, the inherent risk to personnel in the AIT facilities prevent about the use of laser in the free space.

The detectors are PIN silicon photodiodes, which can detect radiation in all three wavelengths. Therefore, a system that allows the detectors on each channel to be sensitive only to their wavelength must be implemented. One common option is the use of interferential filters. Detectors in the lower channel (660 nm) were made of a low-pass filter with a nominal cutoff wavelength of 720 nm, placed over the photodiodes. High-pass filters with a nominal cutoff wavelength of 880 nm were placed over the photodiodes of the high channel. Detectors in the middle channel had band-pass filters.

If light inside the spacecraft were always to arrive nearly perpendicular to the detectors ($\pm 10°$), then WDMA techniques would be trivial to implement. It would only be necessary to find band-pass filters narrow enough to allow the coexistence of the n channels in the selected wavelength band. But one of the main characteristics of interferential filters is the variation of their transmittance window when light does not arrive perpendicularly to their surface. The displacement of the transmittance maximum follows this formula [16]:

$$\lambda_\theta = \lambda_0 \left[1 - \left(\frac{n_e}{n^*} \right)^2 \sin^2 \theta \right] \tag{16}$$

where λ_θ being the maximum transmittance wavelength under an incidence at angle θ, λ_0 the maximum transmittance wavelength under normal incidence, n_e the refractive index for the external medium, and n^* the effective refractive index for the interferential filter. The final results when the incidence is in the range $(-\pi/2, \pi/2)$ is a widening of the transmittance band of the filter and a displacement of the transmittance maximum to lower wavelengths, together with a decrease of the maximum transmittance value, as can be seen in Fig. 9. This figure represents the experimental responsivities of a Si photodiode (S5106 of Hamamatsu/25 mm^2 of active area) with an interference filter centered in 805 nm and with 40 nm of full width at half maximum that is illuminated under quasi-monochromatic light (monochromator with slits to achieve $\Delta\lambda = 10$ nm, to have optical power enough). Each curve represents the responsivity for an incident angle, between 0° and 70° (over this value the detection system had no sensitivity). The apparent shift of the maximum at 0° from 805 nm to 790 nm, and the elbows in the 0°, 5°, 10° curves, has no physical significance in our experiment, because they are due to the monochromator bandwidth (it has its upper limit at 840 nm and this affects to the measured spectral signal).

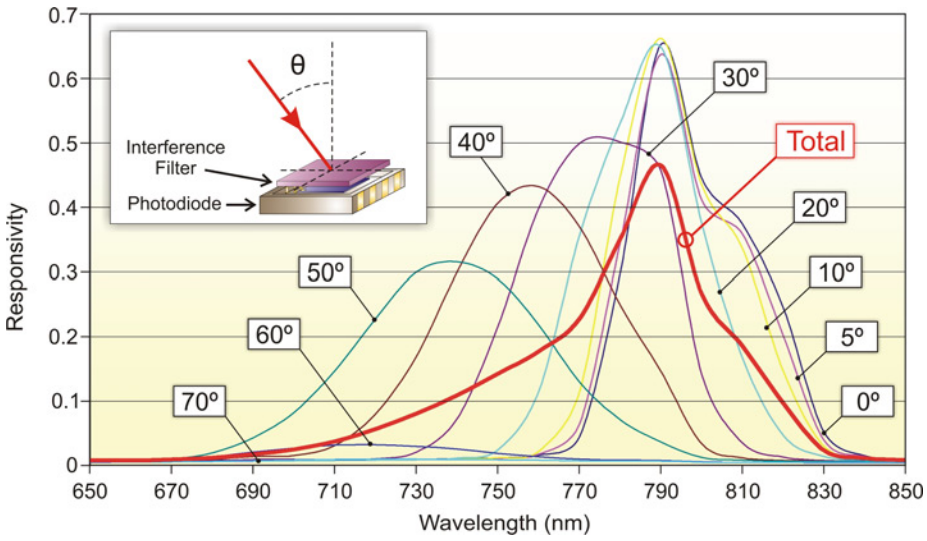

Fig. 9 Responsivity of a detector under uniform diffuse light ("Total" curve in the figure) can be expressed as a sum of all the components of responsivity as a function of angle. Contributions at 80° and 90° were under the detectors threshold. Greater angles are responsible for the "Total" viewing window broadening.

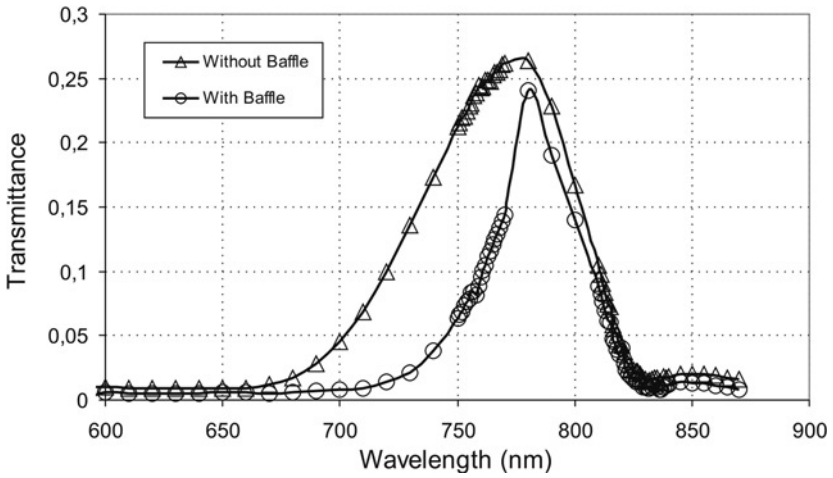

Fig. 10 Responsivity for a photodiode + filter system under uniform light (an integrating sphere was used). Spectrum of detection narrows dramatically when a baffle is added (27 mm height; aperture ±30°), without great losses in the total power received.

As it can be seen in Fig. 9, the transmission spectrum of the filter is shifted to low wavelengths, as stated in (16). The fall in transmittance is due to the Fresnel reflection. The "Total" response curve was measured by placing the photodiode with the filter at the output of an integrating sphere, that is, under diffuse illumination. Note that the total spectral transmittance of the photodiode with the filter for diffuse light suffers a nonnegligible penalty.

The main problem associated with WDMA is the overlapping of channel signals. Due to the displacement of the transmittance bands for the filters, as shown in Fig. 9, part of the radiation emitted in one channel can be detected by another one, thus causing a SNR increase that can lead to errors in communications. The first method to be used to avoid this mutual detection between channels can be the use of optical baffles, which limits the field of view of the photodiodes-filter devices, so that higher angles of incidence are blocked. Although the total received power decreases, improvement in the width of detection bands increases the SNR for all channels. A result for baffle use can be seen in Fig. 10. A 27 mm height baffle (25 mm inner diameter, with aperture ±30°). The advantage of limiting the high-angle degrees has a penalty in the optical power received, but undoubtedly has an advantage in maintaining the bandwidth. With this kind of solutions, the OWLS can be successfully implemented in spacecrafts environments to multiplex at least three wavelengths, using common emitters as 660, 810, and 950 nm.

IV. Detectors

Another problem we faced was power budget. It is not only necessary to separate channels, but also to ensure that every detector receives enough power from the associated emitter(s). The most basic configuration for a detector is a photodiode with an interferential filter over it. When this detector is placed in an area of the satellite where arriving power is insufficient and it is not possible—for operational reasons—to change its location, there are several ways to increase the power budget for that detector. One of the simplest ways is by placing a hemispherical lens that increases the effective area of the photodiode. In the first tests, the photosignal increased by about 80% on average. This was done with Hamamatsu Photodiodes S5106 (25 mm^2 active area) with a 6 mm diameter hemispherical lens placed on them. The measurement setup was at the output of an integrating sphere, and the 80% of signal increase was measured with and without the lens.

The main problem with lenses was the need of using an index matching fluid for the lens and the photodiode. Without it, lens losses caused by reflection in the air interphase between the lens and the photodiode were greater than the gains. The use of an index matching fluid is not a simple issue in Space because of outgassing in space environments. In fact, for final use in Space a transparent epoxy resin is used instead of the index matching fluid. Given that there are many resins qualified for Space use that do not outgas and do not lose transmittance with radiation, we can consider that the use of lenses constitutes an advantage without drawbacks, except for a small increase in

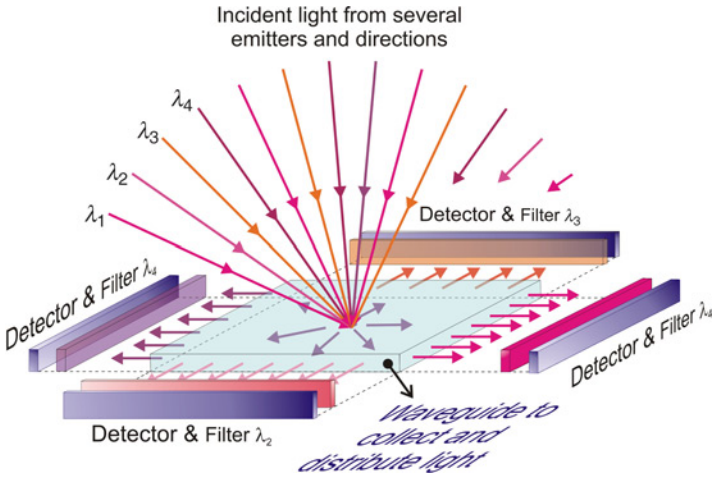

Fig. 11 A solution to improve optical power detection is to use a transparent plate to collect light. The light inside the plate can be transmitted in some way by total internal reflection, as happens in solar energy plate collectors. Besides, if this plate has a waveguide structure, the output angle of the light can be reduced, and interference filters placed in front of detectors can work under low-angle incidence.

payload weight, negligible if compared with the weight reduction achieved by eliminating communication cables and connectors. However, with this solution, the volume increases and flat packaging is lost.

Other setups based on optical elements are under study. The attempt to build a waveguide from a simple material, as a transparent plate is being developed. The intention is to increase the available surface by inducing total reflection inside a transparent sheet, with the detectors placed on its edges. This system provided two advantages. On the one hand, the light collection surface would be greatly increased. On the other hand, if a waveguide structure is made inside the plate, light arriving to the detectors would have very little angular variation, which would increase the efficiency of the interferential filters. A schematic view of one of such systems is showed in Fig. 11.

Simulations and tests on standard plates with microprisms to collect light showed that almost no radiation was forced into total reflection; but more advanced devices based on holography and waveguides promise better results. The incorporation of fluorescent dopants is also under study, even by forming a waveguide with active fluorescent materials inside them. This solution tries to avoid the use of larger photodiodes. These are not an option, since parasitic capacity increases with size, which forces unacceptable restraints on the OWLS payload electronics due its negative effect on the bandwidth.

V. Conclusions

In numerical and analytical calculations, it can be seen that even in a very simple geometric environment, and taking into account only one rebound for propagating radiation, dramatic differences appear between different model predictions for power and system bandwidth. In order to obtain reliable results when simulating intra-spacecraft environments, the use of an appropriate reflection model is mandatory. Aluminized Kapton was characterized and classified as non-Lambertian. As a great majority of materials used in space applications exhibit non-Lambertian behavior, it is necessary to use more advanced reflection models when dealing with space optical wireless applications.

In the design stage of a wireless optical communications system, it is mandatory to rely on an accurate description of the behavior of the materials in the channel. The Phong model is able to approximate the angular reflection behavior for most space materials. Nevertheless, other materials can be simulated in a better way by using more complex models, such as the Harvey model for metals or, in the case of mechanized aluminum, by a conical diffraction model [17].

As a first step towards increasing received power in the detectors, lenses were placed over the detectors. This increased their effective area and the received power increased by a factor of around 1.8. Lenses contribute both to

increasing the photodetection signal and to the separation of channels in WDMA. This makes them very important items for intra-spacecraft optical communications.

WDMA can be improved by using simple optical elements, such as optical baffles or lenses. An optical baffle reduces spectral width of detection for photodiode + interferential filter systems, allowing for a greater separation between optical channels and lower SNR, without losing a significant amount of power.

Acknowledgments

R.T. and J.J.J. acknowledge INTA for financing their PhD Theses through a "Calvo Rodés" grant. This work has been partially financed by the Spanish Ministry for Science and Innovation (MICINN) through Projects: Optomag-Mantis (ESP2005–05278) and nanoLambda (NAN2004–09317-C04-03).

References

[1] Gfeller, F. R., and Bapst, U., "Wireless In-house Data Communication via Diffuse Infrared Radiation," *Proceedings of the IEEE*, Vol. 67, 1979, pp. 1474–1486.
doi: 10.1109/PROC.1979.11508

[2] Barry, J. R., Kahn, J. M., Lee, E. A., and Messerschmitt, D.G., "High-Speed Nondirective Optical Communication for Wireless Networks," *IEEE Network Magazine*, Nov., 1991, pp. 44–54.
doi: 10.1109/65.103810

[3] Guerrero, H., Arruego, I., Álvarez, M. T., Álvarez, A., Rodríguez, S., Torres, J., Santamaría, A., and López-Hernández, F. J., "Optical Wireless Links for intra-Satellite Communications (OWLS): The Merger of Optoelectronic and Micro/Nano-technologies," *NanoTech 2002—At the Edge of Revolution*. AIAA, Reston, VA, Sept. 2002.

[4] Gayrard, J. D., Maignan, M., Sotom, M., Benazet, B., and Venet, N., "Applications of Optical Techniques in Future Communication Payloads," *21st International Communications Satellite Systems Conference and Exhibit*, AIAA, Reston, VA, 2003.

[5] Arruego, I., Guerrero, H., Rodríguez, S., Martínez-Oter, J., Jiménez, J. J., Domínguez, J. A., Martín-Ortega, A., de Mingo, J. R., Rivas, J., Apéstigue, V., Sánchez, J., Iglesias, J., Álvarez, M. T., Gallego, P., Azcue, J., Ruiz de Galarreta, C., Martín, B., Álvarez-Herrero, A., Díaz-Michelena, M., Martín, I., Tamayo, F. R., Reina, M., Gutiérrez, M. J., Sabau, L., and Torres, J., "OWLS: A Ten-year History in Optical Wireless Links for intra-Satellite Communications," *IEEE Journal on Selected Areas in Communications*, Vol. 27, No. 9, Dec., 2009, pp. 1599–1611.

[6] Kahn, J. M., and Hoch, J. S., "Simulation Tools for Free-Space Optical Interconnects Based on Computer-generated Holograms," *LEOS 1993 Summer Topical Meeting Digest on Optical Microwave Interactions/Visible Semiconductor Lasers/Impact of Fiber Nonlinearities on Lightwave Systems/Hybrid Optoelectronic Integration and Packaging/Gigabit Networks*, Santa Barbara, CA, pp. 45–46.

[7] Feldman, M. R., and Guest, C. C., "Computer Generated Holographic Optical Elements for Optical Interconnection of Very Large Scale Integrated Circuits," *Applied Optics*, Vol. 26, 1987, pp. 4377–4384.
doi: 10.1364/AO.26.004377

[8] Haney, M. W., and Christensen, M. P., "Performance Scaling Comparison for Free-Space Optical and Electrical Interconnection Approaches," *Applied Optics*, Vol. 37, 1998, pp. 2886–2894.
doi: 10.1364/AO.37.002886

[9] Lopez-Hernandez, F. J., Perez-Jimenez, R., and Santamaria, A., "Modified Monte Carlo Scheme for High-Efficiency Simulation of the Impulse Response on Diffuse IR Wireless Indoor Channels," *Electronics Letters*, Vol. 34, 1998, pp. 1819–1820.
doi: 10.1049/el:19981173

[10] Kahn, J. M., Krause, W. J., and Carruthers, J. B., "Experimental Characterization of Non-directed Indoor Infrared Channels," *IEEE Transactions on Communications*, Vol. 43, 1995, pp. 1613–1624.
doi: 10.1109/26.380210

[11] Phong, B. T., "Illumination for Computer Generated Pictures," *Communications of the ACM*, Vol. 18, 1975, pp. 311–317.
doi: 10.1145/360825.360839

[12] Lewis, R., "Making Shaders More Physically Plausible," *Computer Graphics Forum*, Vol. 13, 1994, pp.109–120.
doi: 10.1111/1467-8659.1320109

[13] Minnaert, M., "The Reciprocity Principle in Lunar Photometry," *Astrophysical Journal*, Vol. 93, 1941, pp. 403–410.
doi: 10.1086/144279

[14] Drolen, B. L., "Bidirectional Reflectance and Surface Specularity Results for a Variety of Spacecraft Thermal Control Materials," *AIAA 26th Thermophysics Conference*, AIAA, Washington, DC, June 1991.

[15] Ghisoni, M., Bengtsson, J., Vukusic, J. A., Martinsson, H., and Larsson, A., "Single- and Multimode VCSELs Operating with Continuous Reliefkinoform for Focussed Spot-Array Generation," *IEEE Photonic Technology Letters*, Vol. 9, 1997, pp. 1466–1468.
doi: 10.1109/68.634710

[16] Saurel, J. M., and Roig, J., "Properties of Fabry–Perot Interferential Filters Illuminated in Oblique Incidence," *Journal of Optics*, Vol. 10, 1979, pp. 179–193.
doi: 10.1088/0150-536X/10/4/004

[17] Berry, M. V., Jeffrey, M. R., and Lunney, J. G., "Conical Diffraction: Observations and Theory," *Proceedings of the Royal Society of London, Series A*, Vol. 462, 2006, pp. 1629–1642.

Christopher Rouff
Associate Editor